Nanoscale

ROYAL SOCIETY OF CHEMISTRY

PAPER

View Article Online
View Journal | View Issue

Cite this: *Nanoscale*, 2024, **16**, 11126

A natural killer T cell nanoagonist-initiated immune cascade for hepatocellular carcinoma synergistic immunotherapy†

Ting Luo,‡[a,b,c] Xiaoqiong Tan,‡[c] Guangchao Qing,[c] Jie Yu,*[b] Xing-Jie Liang *[c,d] and Ping Liang *[a,b]

Natural killer T (NKT) cell-mediated immunotherapy shows great promise in hepatocellular carcinoma featuring an inherent immunosuppressive microenvironment. However, targeted delivery of NKT cell agonists remains challenging. Here, we developed a hyaluronic acid (HA) modified metal organic framework (zeolitic imidazolate framework-8, ZIF-8) to encapsulate α-galactosylceramide (α-Galcer), a classic NKT cell agonist, and doxorubicin (DOX) for eliminating liver cancer, denoted as α-Galcer/DOX@ZIF-8@HA. In the tumor microenvironment (TME), these pH-responsive nano-frameworks can gradually collapse to release α-Galcer for activating NKT cells and further boosting other immune cells in order to initiate an antitumor immune cascade. Along with DOX, the released α-Galcer enabled efficient NKT cell activation in TME for synergistic immunotherapy and tumor elimination, leading to evident tumor suppression and prolonged animal survival in both subcutaneous and orthotopic liver tumor models. Manipulating NKT cell agonists into functional nano-frameworks in TME may be matched with other advanced managements applied in a wider range of cancer therapies.

Received 28th February 2024,
Accepted 13th May 2024

DOI: 10.1039/d4nr00847b

rsc.li/nanoscale

1. Introduction

Worldwide, hepatocellular carcinoma (HCC) is one of the leading causes of death and it often results in a very poor five-year survival rate.[1] Owing to insidious clinical manifestation, the majority of patients progress into an advanced stage where curative treatments, such as hepatectomy, interventional ablation, and liver transplantation, are not an option.[2,3] Recently, immunotherapies have emerged and have changed the landscape of systemic treatment for advanced HCC.[4,5] The clinical efficacy of those immunotherapies is often hindered by intrinsic tumor heterogeneity and immune tolerance in HCC.[6,7] Therefore, more efficient strategies are highly desirable for remodelling the tumor microenvironment (TME) to immunoactivated status against HCC.

Natural killer T (NKT) cells are a subgroup of innate-like T cells that share similar functions and phenotypes with both NK cells and T cells, which are rising stars in cancer immunotherapy.[8,9] Even though the number of tumor infiltrated NKT cells is far less than that of conventional $CD8^+$ T cells and NK cells, NKT cells exhibit rapid and abundant cytokine production leading to potent and direct cytotoxic T lymphocyte-like antitumor immunity.[10] Additionally, activated NKT cells can further enhance NK cells, $CD8^+$ T cells, and dendritic cells (DCs) for reshaping the immune environment into a "hot tumor".[11–14] So, it is critical to directly and efficiently bridge both adaptive and innate immunity initiated by NKT cells. α-Galactosylceramide (α-Galcer), an exogenous glycolipid, represents a classic major histocompatibility complex class-I like molecule CD1d-restricted agonist, which needs to be delivered to NKT cells.[15] As previously reported, NKT cell-based immunotherapy controled liver cancer in a preclinical study.[16,17] Adoptive transfer of α-Galcer-pulsed DCs also inhibited liver metastasis in an NKT cell-dependent manner.[18] However, α-Galcer has poor water solubility and a short half-life in biological conditions, which lead to unsatisfactory medical application.[19] Of note, NKT cells possess a tissue-resident nature instead of being recruited from lymph nodes through peripheral circulation.[20] Therefore, an instant delivery strategy of α-Galcer is of great significance for *in situ* NKT cell activation.

Due to their high porosity and structural adjustability, metal organic frameworks (MOFs), a subset of coordination

[a]*School of Medicine, Nankai University, Tianjin, 300071, China. E-mail: liangping301@hotmail.com*
[b]*Department of Interventional Ultrasound, Fifth Medical Center of Chinese People's Liberation Army General Hospital, Beijing, 100853, China. E-mail: jiemi301@163.com*
[c]*CAS Key Laboratory for Biomedical Effects of Nanomaterials and Nanosafety, CAS Center for Excellence in Nanoscience, National Center for Nanoscience and Technology of China, Beijing, 100190, China. E-mail: Liangxj@nanoctr.cn*
[d]*University of Chinese Academy of Sciences, Beijing 100049, China*

†Electronic supplementary information (ESI) available. See DOI: https://doi.org/10.1039/d4nr00847b

‡These authors contributed equally to this work.

polymers built from metal ions or clusters and organic linkers, have drawn considerable attention in the field of drug delivery.[21] In the whole MOF family, zeolitic imidazolate framework-8 (ZIF-8) is the most attractive drug delivery nanosystem with high biocompatibility and pH-responsive degradability.[22,23] Mild acidity is the main feature of TME, promoting the proliferation, angiogenesis, and metabolism of tumor cells.[24] Consequently, it is important to utilize ZIF-8 as a versatile delivery carrier in drug encapsulation and acid-responsive drug release for tumor suppression.[25] Moreover, ZIF-8 can be prepared through a simple one-pot synthesis with small molecule drugs to form nanoparticles (NPs) with uniform size.[26,27]

Accordingly, we prepared hyaluronic acid (HA)-modified ZIF-8 nanoagonists for *in situ* NKT cell activation in order to achieve enhanced antitumor immunotherapy together with DOX. As shown in Scheme 1, the NPs were manufactured by simultaneously encapsulating α-Galcer and DOX into the ZIF-8 assembly, then adding the HA coating outside, denoted as α-Galcer/DOX@ZIF-8@HA. The results showed that α-Galcer/DOX@ZIF-8@HA can efficiently accumulate in the tumor and then the ZIF-8 framework disassembles, releasing the cargoes of α-Galcer and DOX in the TME. Once NKT cells were activated *via* α-Galcer presented by DCs, a large amount of IFN γ was produced and caused potent cytotoxicity, which further primed other immune cells including NK cells and $CD8^+$ T cells to fight against the tumor. Thereby, the reversal of immunosuppressive TME and DOX cytotoxicity both contributed to the overall antitumor effect. This excellent immunotherapeutic effect has been confirmed in both a subcutaneous Hepa1–6 tumor model and a diethylnitrosamine-carbon tetrachloride ($DEN\text{-}CCl_4$) induced orthotopic liver tumor model. Our findings may provide an inspiration for enhanced immunotherapy of HCC.

2. Materials and methods

2.1. Materials

$Zn(NO_3)_2{\cdot}6H_2O$ and 2-methylimidazole were purchased from Alfa Aesar (Beijing, China). α-Galactosylceramide was produced by MedChemExpress (Shanghai, China). Doxorubicin HCl

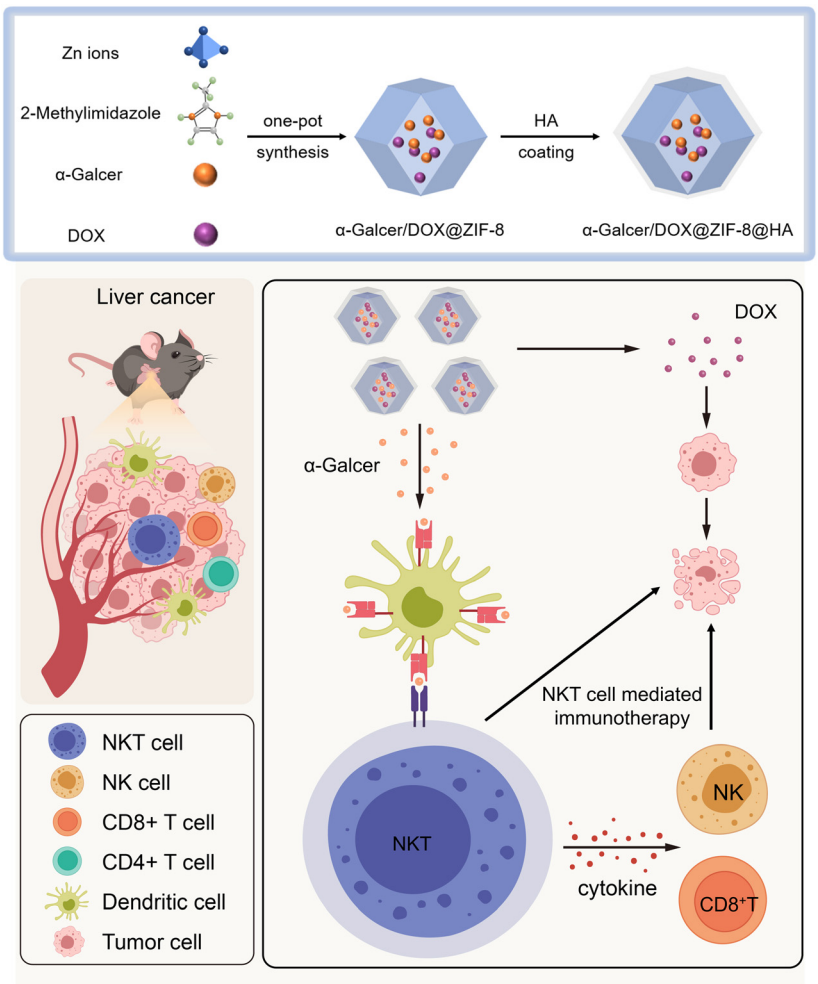

Scheme 1 Schematic diagram of α-Galcer/DOX@ZIF-8@HA synthesis and NKT cell-mediated synergistic immunotherapy.

(DOX) was obtained from Meilunbio (Dalian, China). Hyaluronic acid (HA) and carbon tetrachloride (CCl_4) were obtained from Macklin (Shanghai, China). Diethylnitrosamine (DEN) was purchased from Sigma-Aldrich (Munich, Germany). Olive oil was obtained from Solarbio (Beijing, China). The tetramer (PE-mouse CD1d PBS-57), used to NKT cell staining in flow cytometry, was obtained from the NIH Tetramer Core Facility. All chemicals were of analytical grade and used as received.

2.2. Synthesis and characterization of α-Galcer/DOX@ZIF-8@HA

The α-Galcer/DOX@ZIF-8 was prepared by one-pot synthesis. Typically, 0.2 g of $Zn(NO_3)_2{\cdot}6H_2O$ (dissolved in 2 mL of deionized water) and 0.02 g of DOX (dissolved in 2 mL of deionized water) were mixed together. Then 0.001 g of α-Galcer (dissolved in 1 mL of methanol) and 0.6 g of organic linker 2-methylimidazole (dissolved in 6 mL of deionized water) were added dropwise to the above mixed solution. The total solution was alkalized to pH = 8 and stirred vigorously and constantly for 30 min at room temperature. The products were centrifuged (10 000 rpm for 10 min) and washed three times. Finally, the obtained products were lyophilized for further usage. The synthesis protocols of DOX@ZIF-8 and α-Galcer@ZIF-8 are consistent with the above method. Next, 50 mg of α-Galcer/DOX@ZIF-8 was added to 50 mL of 0.5 mg mL^{-1} HA aqueous solution and stirred for 12 h at room temperature. The products were centrifuged (10 000 rpm for 10 min) and washed three times. Finally, the obtained α-Galcer/DOX@ZIF-8@HA was lyophilized for further usage.

The morphology and structure of NPs were analyzed by transmission electron microscopy (TEM, HT7700, Hitachi Ltd, Tokyo, Japan). Scanning electron microscopy (SEM) and energy dispersive X-ray spectroscopy (EDS) (ZEISS GeminiSEM 300) were performed at an accelerating voltage of 200 kV. The hydrodynamic diameters of nanoparticles in water or DMEM medium were characterized by dynamic light scattering (DLS, Zetasizer Nano ZS, Malvern PANalytical Ltd, UK). The UV-vis absorption spectra of ZIF-8, DOX, DOX@ZIF-8, DOX@ZIF-8@HA, and α-Galcer/DOX@ZIF-8@HA were recorded using a UV-vis spectrophotometer (Lambda-950, PerkinElmer Instruments Co., Ltd, USA). Fourier transform infrared (FT-IR) spectra were recorded on a FT-IR spectrometer (Nicolet iS20, Thermo Fisher Scientific, USA). X-ray diffraction (XRD) patterns were collected on a D/MAX-TTRIII (CBO) X-ray diffractometer (Rigaku Corporation, Japan) equipped with Cu Kα radiation (λ = 1.542 Å).

2.3. *In vitro* pH-sensitive drug release

The drug release profile of α-Galcer/DOX@ZIF-8@HA was studied using dialysis tubes (T-O-Dialyzer, 3.0 KD, Sangon Biotech) and a shaking incubator. The obtained α-Galcer/DOX@ZIF-8@HA NPs were suspended in a 2 mL PBS solution in dialysis tubes. All dialysis tubes were immersed in a 35 mL buffer at different pH values (5.5, 6.5, and 7.4) and shaken at a rate of 200 rpm at 37 °C for 24 h. The supernatant (3 mL) was collected at each scheduled time (0.5, 3, 5, 7, 9, 12, and 24 h) and replaced by the same volume of buffer. High-performance liquid chromatography–tandem mass spectrometry and fluorescence spectrophotometry were used to determine the amount of released drug. This release experiment of the drug was carried out in triplicate.

$$\text{Release percentage of drug } (\%) = M_r/M_l \times 100\%$$

where M_r and M_l are the total mass of drug released and loaded, respectively.

2.4. Cell lines

Hepa1–6, HepG2, and WRL68 cell lines were purchased from the American Type Culture Collection and cultured in a 5% CO_2 atmosphere at 37 °C. Hepa1–6, HepG2, and WRL68 cells were grown in complete Dulbecco's modified Eagle's medium (DMEM; Gibco, Invitrogen) supplemented with 10% fetal bovine serum (FBS), penicillin (100 U mL^{-1}), streptomycin (100 U mL^{-1}), and 1% L-glutamine, while bone marrow-derived dendritic cells (BMDCs) were cultured in RPMI-1640, supplemented with 10% FBS and 1% penicillin–streptomycin solution.

2.5. *In vitro* cytotoxicity

The cytotoxicity of NPs was evaluated using a Cell Counting Kit-8 assay (CCK-8, Solarbio, China). Hepa1–6, HepG2, and WRL68 cells were seeded in 96-well plates (1×10^4 cells per well) and incubated for 24 h, respectively. The original medium was then replaced with a culture medium containing different concentrations of ZIF-8 (0, 5, 10, 20, 40, 80, and 160 μg mL^{-1}). Subsequently, the cells were incubated with CCK-8 at 37 °C for a further 1 h. The absorbances were measured with a microplate reader at a wavelength of 450 nm. The cell viability of cells only incubated with the culture medium was defined as 100%.

2.6. Hemolysis assay

To obtain erythrocytes, fresh murine blood extracted from C57BL/6 mice was centrifuged at 1000 rpm for 8 min to remove the supernatant and then washed with PBS 4 times. The erythrocyte suspension (10 μL) was added to 90 μL of water as the positive control, 90 μL of PBS as the negative control, and 90 μL of PBS solution containing various compounds, including ZIF-8, DOX@ZIF-8, α-Galcer@ZIF-8, α-Galcer/DOX@ZIF-8, ZIF-8@HA, DOX@ZIF-8@HA, α-Galcer@ZIF-8@HA, and α-Galcer/DOX@ZIF-8@HA NPs (at a concentration of 160 μg mL^{-1}). After incubation at 37 °C for 1 h, samples were centrifuged at 10 000 rpm for 1 min. Photographs of samples were taken and the absorbance of the supernatants at 540 nm was measured using a microplate reader. The hemolysis percentage was calculated using the following formula: hemolysis (%) = $(A_{sample} - A_{PBS})/(A_{water} - A_{PBS}) \times 100\%$, where A_{sample}, A_{PBS} and A_{water} are the absorbances of the sample, PBS and water, respectively.

2.7. *In vitro* NKT cell activation

The BMDCs were isolated from C57BL/6 mice and cultured in medium containing IL-4 and granulocyte/macrophage colony-stimulating factor for 6 days before use. NKT cells ($CD3^+NK1.1^+$) were positively selected from the spleen by fluorescence activated cell sorting (FACS). BMDCs were incubated with PBS, ZIF-8 (35 μg mL^{-1}), free α-Galcer (0.2 μg mL^{-1}), and α-Galcer@ZIF-8 (35 μg mL^{-1}) overnight. Then BMDCs (2×10^4) were washed with PBS and mixed at a ratio of 1 : 2 with NKT cells (4×10^4) for 24 h. Subsequently, cells were collected, washed with PBS, and stained with CD80, CD86, CD69, and tetramer antibody (1 : 100 dilution ratio) at 4 °C for 30 min, and then were assessed by flow cytometry.

2.8. Live/dead cell staining

Hepa1–6 cells (5×10^5 per well) were cultured with DMEM complete culture medium in six-well plates and treated with PBS, ZIF-8 (35 μg mL^{-1}), and α-Galcer/DOX@ZIF-8 (35 μg mL^{-1}). After 24 h of incubation, the medium was removed. Calcein-AM and PI were used for staining cells and observed using a fluorescence microscope.

2.9. *In vivo* tumor targeting studies

Male C57BL/6 mice were subcutaneously injected in the flank with ~5×10^6 Hepa1–6 cells to establish the liver tumor model. When the tumor volume reached 60–100 mm^3, mice were randomly divided into two groups (n = 3): (1) α-Galcer/DOX@ZIF-8; and (2) α-Galcer/DOX@ZIF-8@HA. The NPs were intravenously injected through the tail vein and then monitored using an IVIS Spectrum imaging system (IVIS Spectrum, PerkinElmer, USA) at 2, 4, 8, 12, and 24 h. The tumor and organs were excised for further imaging.

2.10. *In vivo* antitumor studies and immune responses in a Hepa1–6 tumor model

Male C57BL/6 mice were subcutaneously injected in the flank with ~5×10^6 Hepa1–6 cells to establish a liver tumor model. Seven days after tumor inoculation, the tumor volume reached 60–100 mm^3 and then the mice were randomly divided into four groups (n = 6): (1) PBS; (2) α-Galcer@ZIF-8@HA; (3) DOX@ZIF-8@HA; and (4) α-Galcer/DOX@ZIF-8@HA. The doses of α-Galcer and DOX injected *via* the tail vein were both 1 mg per kg body weight. Mice were intravenously injected on the indicated days. The tumor size was measured every four days and the tumor volume was calculated as width^2 × length × 0.5. Mice were sacrificed when the tumor volume reached 1500 mm^3 or when animals became moribund with severe weight loss or ulceration. Next, the tumors and organs including the heart, liver, spleen, lungs, and kidneys were excised, washed with saline, photographed, and finally fixed for histological analysis. H&E and Ki-67 staining tumor tissue were performed according to the manufacturer's instructions. After treatment for 6 days, the blood samples were collected and immediately centrifuged to harvest serum. Blood routine and blood chemistry tests were performed. Then, the tumor and spleen were also isolated to examine the antitumor immune responses. The concentrations of cytokines TNF α and IFN γ in serum were detected by ELISA kits according to the manufacturer's instructions. Subsequently, the NKT cells ($CD3^+$, $NK1.1^+$, $tetramer^+$, $TCR\beta^+$), T cells ($CD45^+$, $CD3^+$, $CD8^+$), and NK cells ($CD3^-$, $NK1.1^+$) were analyzed by flow cytometry.

2.11. *In vivo* antitumor studies in a DEN-CCl_4 induced orthotopic liver tumor model

Male C57BL/6 mice were injected intraperitoneally with diethylnitrosamine (DEN, 25 mg per kg body weight) at 14 days of age, followed by repeated intraperitoneal injections of carbon tetrachloride (CCl_4) (5 μL g^{-1} of an 8 : 2 mixture of olive oil and CCl_4), twice a week, from 8 weeks of age onwards, lasting for 12 weeks. On week 20, the mice were randomly divided into two groups (n = 5): (1) PBS and (2) α-Galcer/DOX@ZIF-8@HA. Mice were intravenously injected on the indicated days. H&E staining, TUNEL (terminal deoxynucleotidyl transferase-mediated deoxyuridine triphosphate nick end labeling) kit staining, Ki-67 staining and immunofluorescence of the $tetramer^+$, $TCR\beta^+$, and $CD8^+$ of tumor tissue were performed according to the manufacturer's instructions.

2.12. Animal ethics statement

All animal experiment operations were conducted in accordance with the "Regulations on the Administration of Laboratory Animals" and guidelines from the National Center for Nanoscience and Technology Animal Health and Use Committee (approval reference number NCNST21-2402-0601). All procedures were performed under inhalation anesthesia using isoflurane.

2.13. Statistical analysis

All data presentation and analysis in this study were carried out using GraphPad Prism 9.0. All data are represented as mean ± standard deviation (s.d.). Statistically different significance between groups were determined using unpaired two-tailed Student's t tests or one-way ANOVA with Dunnett's multiple comparison. The Kaplan–Meier curve and log-rank test were used to analyze the differences in animal survival. $P < 0.05$ was considered statistically significant.

3. Results and discussion

3.1. Synthesis and characterization of α-Galcer/DOX@ZIF-8@HA NPs

As shown in the illustration of Scheme 1, by utilizing pH-responsive ZIF-8 as a nanocarrier, α-Galcer/DOX@ZIF-8 NPs were first synthesized successfully through a one-pot method. We further coated the α-Galcer/DOX@ZIF-8 with HA by electrostatic interaction to improve the biocompatibility and tumor targeting ability. The TEM images and DLS data indicated that the synthesized α-Galcer/DOX@ZIF-8 showed similar octahedral morphology and ~200 nm size to the blank ZIF-8 (Fig. 1a). After coating with HA, the size of α-Galcer/

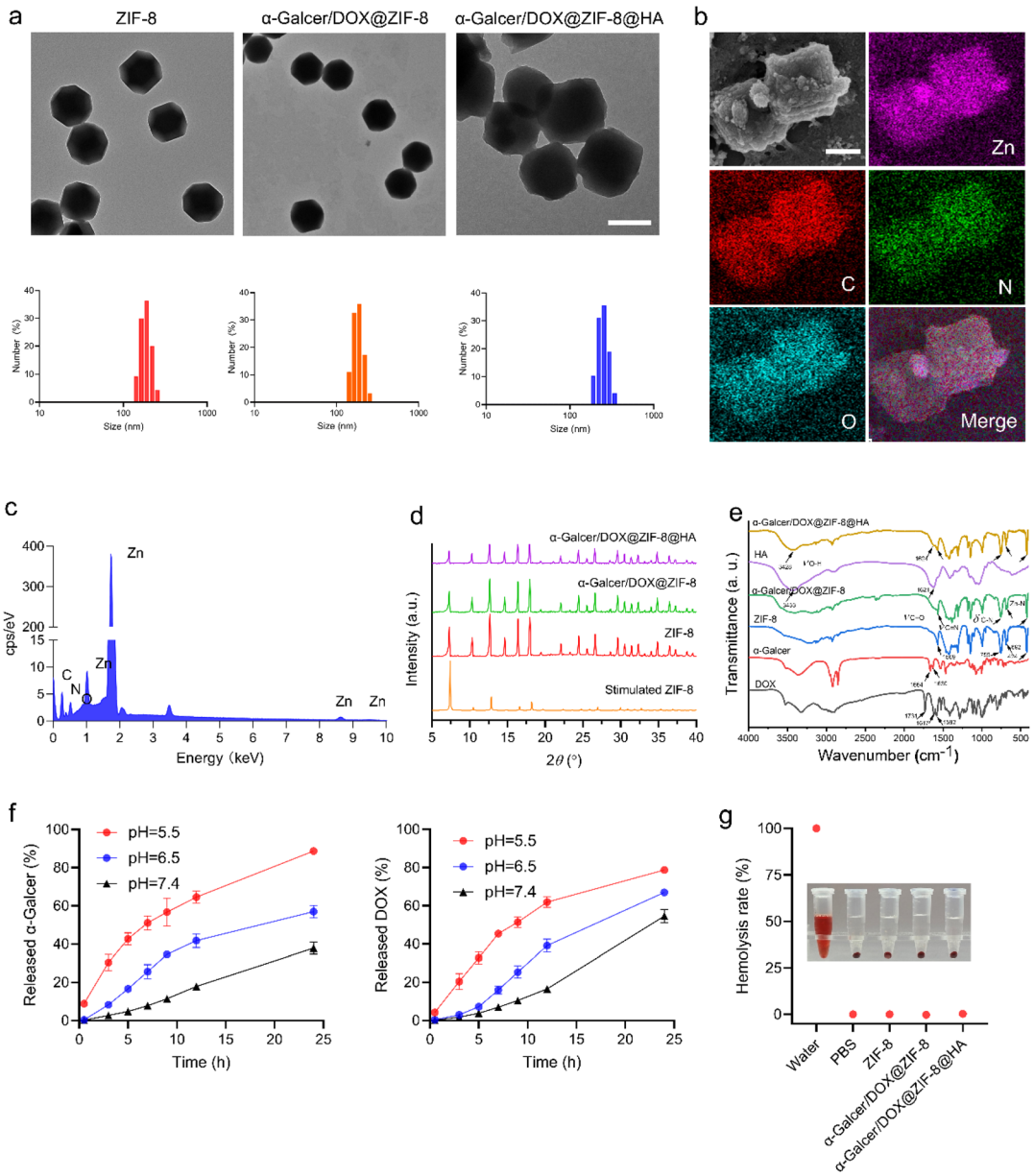

Fig. 1 Characterization of α-Galcer/DOX@ZIF-8@HA. (a) TEM images and hydrodynamic diameters of ZIF-8, α-Galcer/DOX@ZIF-8, and α-Galcer/DOX@ZIF-8@HA NPs in water. Scale bar: 200 nm. (b and c) SEM image of α-Galcer/DOX@ZIF-8@HA, and the corresponding EDS mappings of element distribution, such as zinc (purple), carbon (red), nitrogen (green), and oxygen (blue). Scale bar: 200 nm. (d) XRD patterns of ZIF-8, α-Galcer/DOX@ZIF-8, and α-Galcer/DOX@ZIF-8@HA NPs. (e) FT-IR spectra of DOX, α-Galcer, ZIF-8, α-Galcer/DOX@ZIF-8, HA, and α-Galcer/DOX@ZIF-8@HA. (f) Cumulative release profiles of α-Galcer and DOX from NPs under different conditions. (g) Hemolytic analysis of red blood cells exposed to different formulations.

DOX@ZIF-8@HA increased to 240 nm (Fig. 1a). The TEM images and DLS data of DOX@ZIF-8, α-Galcer@ZIF-8, ZIF-8@HA, DOX@ZIF-8@HA, and α-Galcer@ZIF-8@HA are also shown in Fig. S1.† The HA coating was stable in DMEM for five days (Fig. S2†). The SEM image of α-Galcer/DOX@ZIF-8@HA showed the same nanostructure and size as the TEM image (Fig. 1b). Further elemental mapping of α-Galcer/DOX@ZIF-8@HA showed that zinc, carbon, nitrogen, and oxygen elements were uniformly distributed in α-Galcer/DOX@ZIF-8@HA NPs, which illustrated the successful preparation of homogeneous nano-frameworks (Fig. 1b and c). Powder X-ray diffraction (XRD) analysis indicated that ZIF-8, DOX@ZIF-8, α-Galcer@ZIF-8 and α-Galcer/DOX@ZIF-8@HA, as well as HA-coating NPs, maintained the same highly crystalline structure as stimulated ZIF-8, which implied that the α-Galcer/DOX@ZIF-8@HA was successfully prepared (Fig. 1d and Fig. S3†). The FT-IR spectra of different NPs are displayed in Fig. 1e and Fig. S4,† which show that 758 cm^{-1} and 692 cm^{-1} were both ascribed to out of plane and in plane δ C–N, and the 1569 cm^{-1} was ascribed to ν C=N in the imidazole

ring of 2-methylimidazole. The absorption band at 424 cm^{-1} was ascribed to Zn–N stretching, representing the successful synthesis of ZIF-8. Compared with the FT-IR spectra of ZIF-8, DOX@ZIF-8, α-Galcer@ZIF-8, and α-Galcer/DOX@ZIF-8, all exhibited a wide and weak absorption from 1600 to 1730 cm^{-1}, which might be due to the existing C═O bond of DOX and α-Galcer. After further modification of HA, a new peak at 1624 cm^{-1} occurred and the peak absorption at 3428 cm^{-1} was enhanced. The successful loading of DOX was also confirmed by UV-vis absorption curves and the preparation process did not affect the cargo function (Fig. S5†). The loading efficiencies of DOX in the DOX@ZIF8 and DOX/α-Galcer@ZIF8 were 8.83% and 7.02%, respectively. The loading efficiencies of α-Galcer in the α-Galcer@ZIF8 and DOX/α-Galcer@ZIF8 were 0.56% and 0.47%, respectively (Table S1†).

The pH-responsive drug release of α-Galcer/DOX@ZIF-8@HA was next investigated. The release behavior of α-Galcer/DOX@ZIF-8@HA was studied in PBS (pH = 7.4) and acidic buffers (pH = 6.5 and 5.5), as shown in Fig. 1f. Only 37% of α-Galcer was released in the PBS at pH 7.4 within 24 h. In contrast, 56% of and 88% of α-Galcer were released in the buffer with pH 6.5 and 5.5 within 24 h. The release profile of DOX was similar to that of α-Galcer. This indicated that α-Galcer/DOX@ZIF-8@HA has an improved drug release behavior under acid conditions, which may be attributed to the degradation characteristics of the acidic pH of ZIF-8.[28] Under

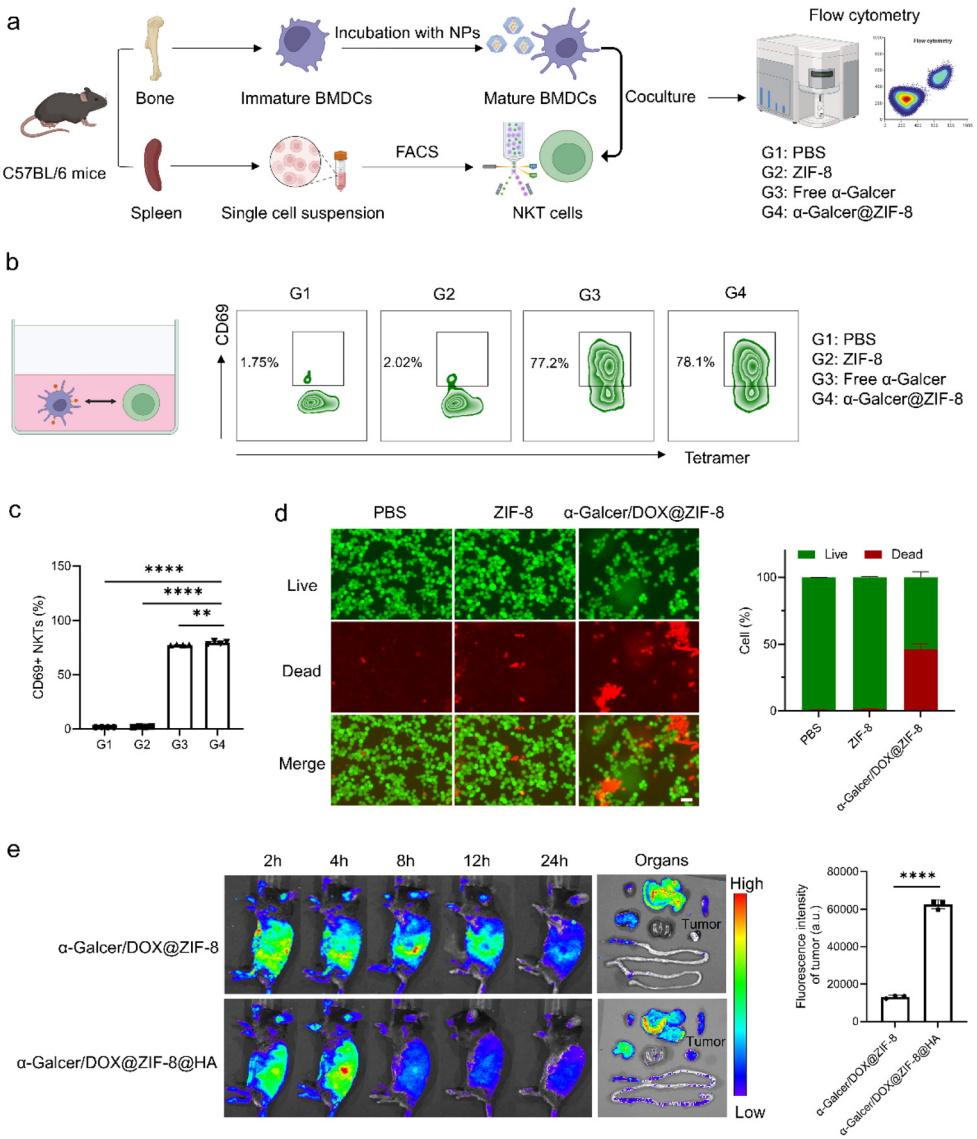

Fig. 2 *In vitro* biological effects and the *in vivo* tumor targeting behavior of α-Galcer/DOX@ZIF-8@HA NPs. (a) Schematic diagram of studying NKT cell activation *in vitro*. (b and c) Flow cytometry and quantitative analysis of NKT cells (n = 4). One-way ANOVA with Dunnett's multiple comparison was used to calculate statistical differences. (d) Fluorescence imaging and quantitative analysis of live/dead cells with different treatments (n = 3). Scale bar: 20 μm. (e) The biodistribution of α-Galcer/DOX@ZIF-8 and α-Galcer/DOX@ZIF-8@HA in the heart, liver, spleen, lungs, kidneys, and tumor at different time points post injection. Two-tailed unpaired Student's t-test was used to calculate statistical differences. * $p < 0.05$; ** $p < 0.01$; *** $p < 0.001$; and **** $p < 0.0001$. Data are presented as mean ± s.d.

acidic environments, organic linkers undergo protonation, leading to the cleavage of the Zn^{2+}-imidazolium metal–ligand bonds and accelerating the degradation of the ZIF-8 structure.[23]

In addition, no obvious hemolysis was observed after the co-incubation of different NPs with red blood cells for 1 h (Fig. 1g and Fig. S6†), showing the high biocompatibility of α-Galcer/DOX@ZIF-8@HA and its components.

3.2. *In vitro* NKT cell activation by α-Galcer/DOX@ZIF-8@HA NPs

We first verified the biosafety of the ZIF-8 nanocarrier in Hepa1–6, HepG2, and WRL68 cells for biomedical application. As shown in Fig. S7,† the cytotoxicity of these cell lines was low and acceptable after 24 h of incubation with ZIF-8 at different concentrations (0, 5, 10, 20, 40, 80, and 160 μg mL^{-1}).

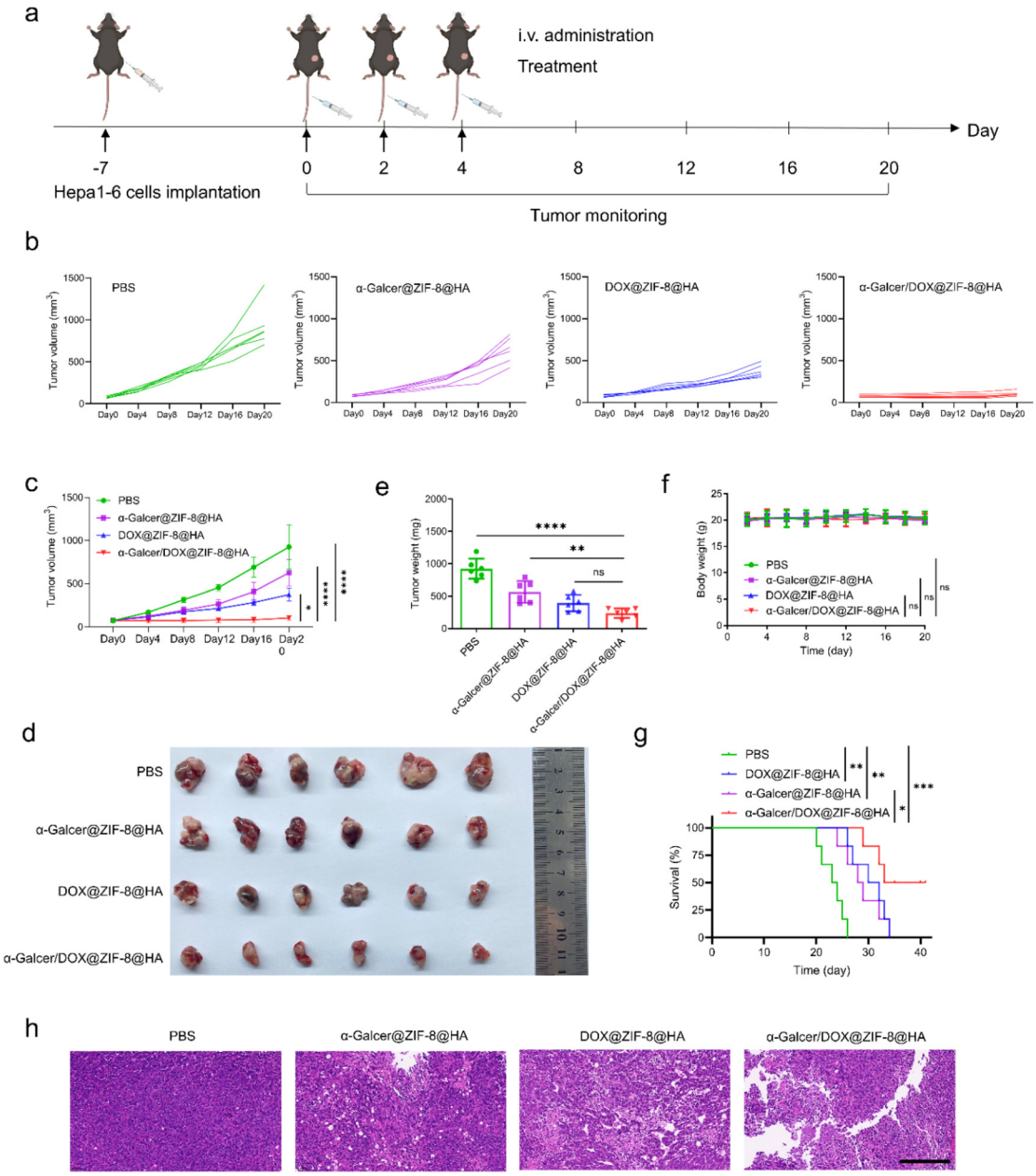

Fig. 3 α-Galcer/DOX@ZIF-8@HA inhibited tumor growth in a subcutaneous Hepa1–6 tumor model. (a) Schematic of the experiment for Hepa1–6 tumor bearing mice. (b and c) Individual tumor growth (b) and the average tumor growth curves (c) of mice from different groups (n = 6). (d) Photographs of tumor tissue from mice treated with different groups. (e–g) The tumor weight (e), mouse body weight changes (f), and survival rate (g) of different groups (n = 6). (h) H&E images of tumor tissue from mice treated with different groups. Scale bar: 200 μm. One-way ANOVA with Dunnett's multiple comparison was used to calculate statistical differences. * $p < 0.05$; ** $p < 0.01$; *** $p < 0.001$; and **** $p < 0.0001$. Data are presented as mean ± s.d.

The ZIF-8 concentration of 160 μg mL^{-1} was further used to evaluate the NKT cell activation. As one of the most crucial antigen presenting cells, DCs expressed CD1d molecule to present α-Galcer to activate NKT cells. With the help of α-Galcer released from NPs, the mature BMDCs upregulated co-stimulatory molecules CD80 and CD86 on the cell surface (Fig. S8†). Next, after co-culture of mature BMDCs and spleen isolated NKT cells, we observed that the activation marker CD69 increased in NKT cells (Fig. 2a–c). Hence, this indicated that α-Galcer@ZIF-8@HA treated BMDCs could potently trigger NKT cell activation. Besides, DOX was added to the ZIF-8 drug delivery nanosystem to determine the cytotoxicity. The results of live/dead staining showed that α-Galcer/DOX@ZIF-8 NPs have confirmed cytotoxicity in Hepa1–6 cells compared with other groups (Fig. 2d).

3.3. *In vivo* tumor targeting behavior

To study the tumor accumulation of α-Galcer/DOX@ZIF-8@HA, the NPs were intravenously injected into Hepa1–6 tumor-bearing mice. Compared with α-Galcer/DOX@ZIF-8, α-Galcer/DOX@ZIF-8@HA displayed evident higher fluorescence signals of DOX in the tumor at 4 h, indicating improved tumor accumulation by virtue of HA-CD44 interaction (Fig. 2e). Moreover, the *ex vivo* fluorescence signals of the isolated tumor and organs were also provided (Fig. 2e). Hence, α-Galcer/DOX@ZIF-8@HA NPs can be accumulated effectively at the tumor site.

3.4. *In vivo* antitumor effect of the α-Galcer/DOX@ZIF-8@HA in a subcutaneous Hepa1–6 tumor model

On the basis of the excellent results *in vitro*, we extended the nanoagonist platform into the subcutaneous Hepa1–6 tumor

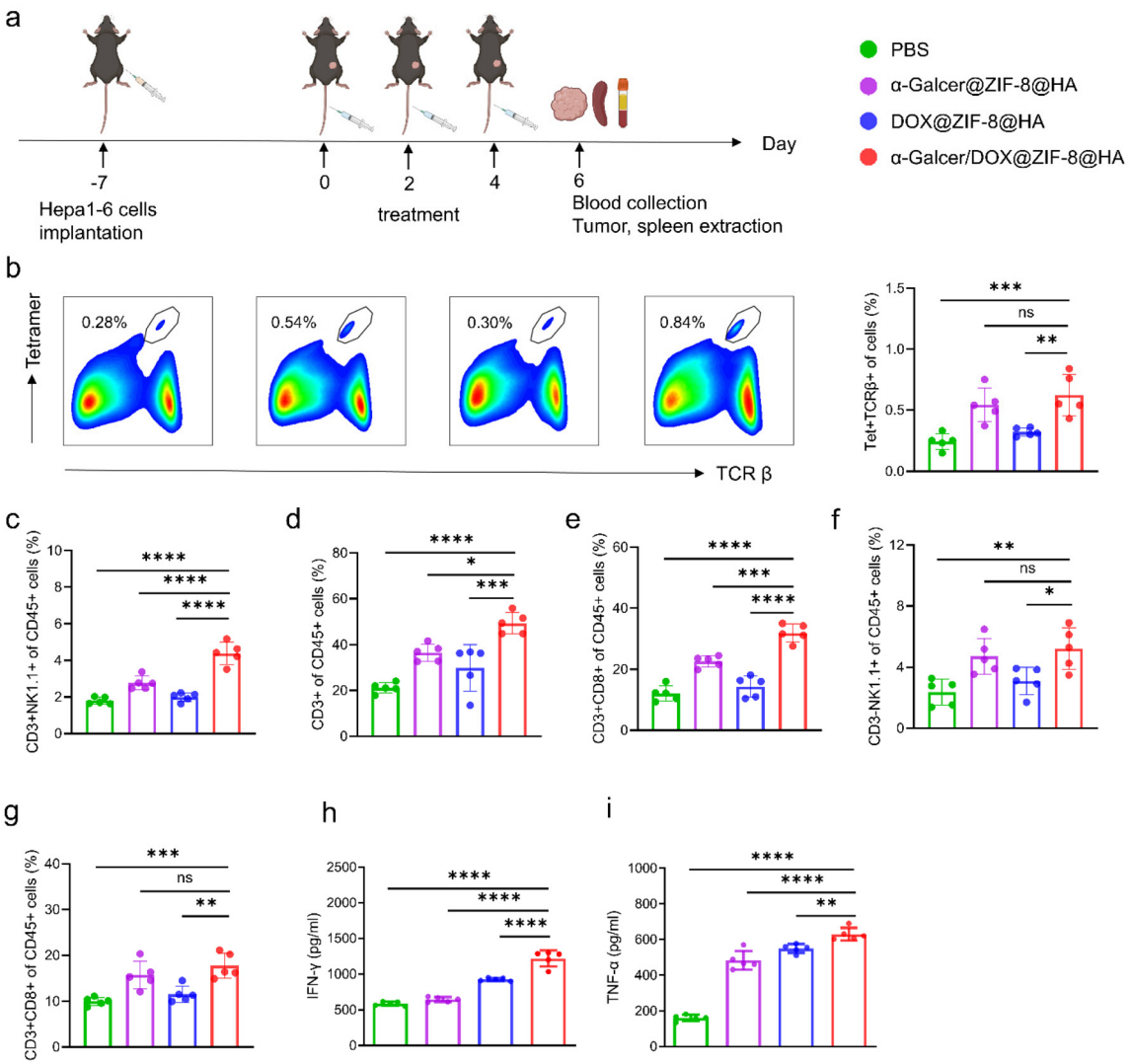

Fig. 4 α-Galcer/DOX@ZIF-8@HA induced antitumor immunity. (a) Schematic diagram of antitumor immunity in Hepa1–6 tumor bearing mice. (b) Flow cytometry and quantitative analysis of tetramer$^+$TCRβ$^+$ NKT cells in tumor tissue (n = 5). (c–f) Quantitative analysis on the populations of tumor-infiltrating CD3$^+$ NK1.1$^+$ NKT cells, total T cells, CD8$^+$ T cytotoxic cells, and NK cells (n = 5). (g) Quantitative analysis on the populations of CD8$^+$ T cells in spleen (n = 5). (h and i) The production of IFN γ (h) and TNF α (i) in serum. One-way ANOVA with Dunnett's multiple comparison was used to calculate statistical differences. * $p < 0.05$; ** $p < 0.01$; *** $p < 0.001$; and **** $p < 0.0001$. Data are presented as mean ± s.d.

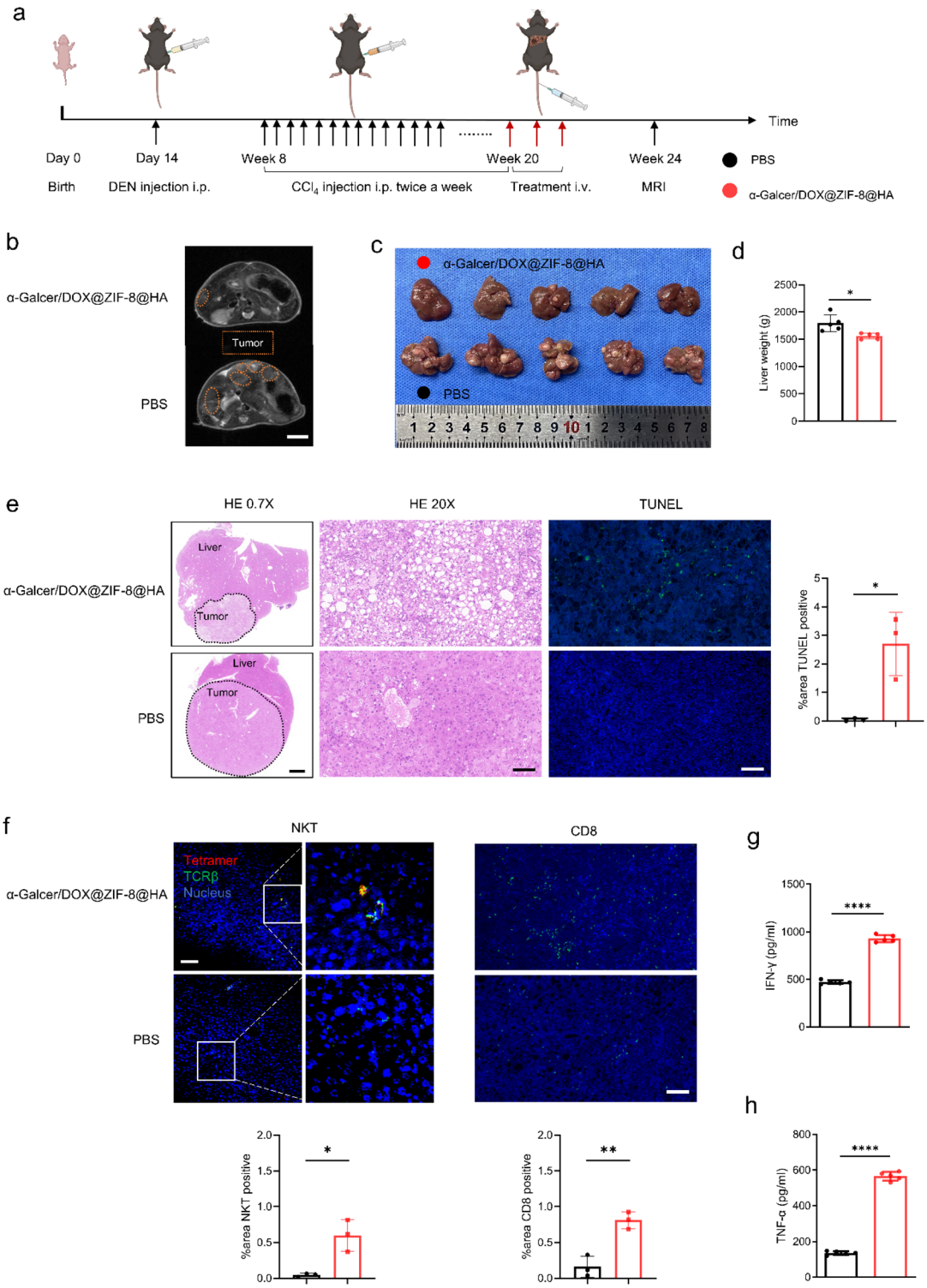

Fig. 5 α-Galcer/DOX@ZIF-8@HA inhibited tumor growth and boosted antitumor immunity in a DEN-CCl_4 induced orthotopic liver tumor model. (a) Schematic diagram of the treatment for a DEN-CCl_4 induced orthotopic liver tumor model. (b and c) MR images (b) and photographs (c) of liver from mice treated with different groups. (d) The liver weights of mice from different groups are shown (n = 5). (e) H&E, TUNEL images (and its quantification) of tumor tissue from mice treated with different groups. Scale bar (from left to right): 2 mm, 100 μm, and 100 μm. (f) NKT cell and CD8 staining (and quantification) of tumor tissue from mice treated with different groups. Scale bar: 100 μm. (g and h) The production of IFN γ (g) and TNF α (h) in serum (n = 5). * $p < 0.05$; ** $p < 0.01$; *** $p < 0.001$; and **** $p < 0.0001$, calculated by two-tailed unpaired Student's t-test. Data are presented as mean ± s.d.

model. When the tumor volume reached approximately 60–100 mm^3, the mice were randomly divided into groups and then PBS, α-Galcer@ZIF-8@HA, DOX@ZIF-8@HA, and α-Galcer/DOX@ZIF-8@HA were injected intravenously. Tumor growth and the survival of mice were recorded every 4 days. α-Galcer/DOX@ZIF-8@HA treatment robustly inhibited the tumor growth and extended the survival of mice, while the mice treated with α-Galcer@ZIF-8@HA and DOX@ZIF-8@HA showed only moderate tumor suppression and a modestly increased survival rate (Fig. 3a–g). Consistently, the excised tumors of the α-Galcer/DOX@ZIF-8@HA group were smaller than those of the other groups (Fig. 3d), which was further demonstrated as the corresponding H&E and Ki-67 staining of tumor tissue (Fig. 3h and Fig. S9†). Together, the above results indicate that α-Galcer/DOX@ZIF-8@HA treatment can inhibit tumor progression.

We also observed that the mice treated with different formulations did not show significant body weight changes (Fig. 3f), suggesting acceptable biosafety. To further evaluate the systemic toxicity of different formulations, serum biochemical assays were performed, including alanine aminotransferase (ALT), aspartate aminotransferase (AST), albumin (ALB), alkaline phosphatase (ALP), and blood urea nitrogen (BUN). The results showed that the serum biochemistry parameters were all at normal levels (Fig. S10†). Blood routine testing also indicated acceptable blood compatibility (Fig. S11†). Histological examination of major organs, including the heart, liver, spleen, lungs, and kidneys, indicated no obvious systemic inflammation or other side effects (Fig. S12†). These data clearly demonstrate the efficacy and safety of α-Galcer/DOX@ZIF-8@HA treatment *in vivo*.

3.5. Antitumor immunity stimulated by α-Galcer/DOX@ZIF-8@HA

To understand the cellular mechanisms underlying the observed immunologic effects, upon treatment, the tumor and spleen were collected and analyzed by flow cytometry (Fig. 4a). As shown in Fig. 4b–f, the immunotherapy considerably promoted α-Galcer specific NKT cell activation and enhanced the intratumoral infiltration of ($CD3^+NK1.1^+$) NKT cells, ($CD3^-NK1.1^+$) NK cells, and ($CD3^+$ and $CD3^+CD8^+$) T cells in the α-Galcer/DOX@ZIF-8@HA group. Additionally, increased T cells ($CD3^+CD8^+$) were observed in the spleen of the α-Galcer/DOX@ZIF-8@HA group (Fig. 4g). α-Galcer/DOX@ZIF-8@HA contributed to effective NKT cell-based immune activation within the TME, and enhanced the levels of proinflammatory cytokines in serum (IFN γ and TNF α) (Fig. 4h and i). Of note, IFN γ is considered as a significant cytokine to trigger a subsequent antitumor immune cascade, especially $CD8^+$ T cells and NK cells.

3.6. *In vivo* antitumor studies in a DEN-CCl_4 induced orthotopic liver tumor model

DEN-CCl_4 induced liver tumors exhibit similar molecular characteristics to human HCC, particularly those associated with high proliferation. Chronic CCl_4 injection (up to 4 months) can lead to liver injury, hepatocyte proliferation, liver fibrosis and cirrhosis, and vascular dysfunction, and form a similar immune microenvironment to that observed in the development of clinical HCC.[29] To reproduce the TME features of HCC, we further established a DEN-CCl_4 induced orthotopic liver tumor model (Fig. 5a). Compared with the PBS group, the α-Galcer/DOX@ZIF-8@HA inhibited the hepatic tumor growth as confirmed by both MR images of the liver (Fig. 5b) and photographs of the excised liver tissue (Fig. 5c). We also weighed the liver and found the smallest tumor of α-Galcer/DOX@ZIF-8@HA among different groups (Fig. 5d). In addition, H&E, Ki-67 and TUNEL staining of hepatic tumors indicated that the α-Galcer/DOX@ZIF-8@HA group showed more effective suppression of tumor growth and induction of tumor apoptosis than the other groups (Fig. 5e and Fig. S13†). In the α-Galcer/DOX@ZIF-8@HA group, the highest recruitment of tetramer$^+$TCRβ$^+$ NKT cells (Fig. 5f) and the highest levels of IFN γ (Fig. 5g) and TNF α (Fig. 5h) were also found in hepatic tumors, indicating its excellent *in vivo* ability to mediate NKT cell activation for the strongest immune response. Immunofluorescence analysis demonstrated that α-Galcer/DOX@ZIF-8@HA significantly increased $CD8^+$ T cell infiltration in tumors (Fig. 5f). Together, these results indicate that α-Galcer/DOX@ZIF-8@HA treatment can inhibit tumor progression and arouse antitumor immunity in the orthotopic model.

We also performed a safety study in this model to ensure biocompatibility. The results of body weight changes (Fig. S14†), serum biochemical assay (Fig. S15†), and H&E examination of major organs (Fig. S16†) totally confirmed that α-Galcer/DOX@ZIF-8@HA treatment did not cause serious adverse events in the mice.

Compared with previous studies regarding other drug delivery systems such as liposomes, Dewitte's group[30] developed mRNA Galsomes to codeliver nucleoside-modified antigen-encoding mRNA and the glycolipid antigen and α-Galcer to antigen presenting cells. This liposome does not have any smart responsive abilities, while our ZIF-8 nanocarrier has an acid-responsive drug release profile. Besides, without delivering α-Galcer to activate NKT cells *in situ*, Yucai Wang *et al.*[16] used photothermal therapy to promote the antitumor ability of adoptively transferred NKT cells. Considering the high cost of *in vitro* cell proliferation and *in vivo* tumor targeting of adoptive cells, our strategy may be a better way to enhance the antitumor immunity of NKT cells.

4. Conclusions

In summary, we developed HA-functionalized ZIF-8 nanoagonists for *in situ* enhancing synergistic NKT cell-based immunotherapy. The novel nanoplatform not only served as a carrier for packaging, tumor accumulation, and controlled release of α-Galcer to boost intratumoral resident NKT cells, but also was able to induce antitumor efficacy *via* cytotoxic T cells and NK cells, together with DOX chemotoxicity. It is demonstrated that

α-Galcer/DOX@ZIF-8@HA triggered efficient antitumor immune responses and prolonged survival in both subcutaneous and orthotopic liver tumor models. This work presents a promising strategy to reshape the tumor immune microenvironment and to overcome the current obstacles to potent NKT cell-based immunotherapy for liver cancer.

Author contributions

X.-J. Liang and P. Liang designed the project. T. Luo and X. Tan completed the experiments. T. Luo, X. Tan and G. Qing collected the data, T. Luo and X. Tan analysed the data. T. Luo, X. Tan and G. Qing wrote the manuscript. P. Liang, J. Yu and X.-J. Liang supervised the project.

Conflicts of interest

There are no conflicts to declare.

Acknowledgements

This work was supported by the National Key Research & Development Program of China (grant no. 2021YFA1201000), the National Natural Science Foundation of China (NSFC) major research plan (grant no. 92159305), NSFC key project (grant no. 32030060), and the NSFC international collaboration key project (grant no. 51861135103). The authors also appreciate the support by "the Chinese Academy of Sciences (CAS-NSTDA) International Partnership Program" (121D11KYSB20210003) and Strategic Priority Research Program of Chinese Academy of Sciences (XDB36000000). Some flow and schematic diagrams contain elements from Biorender (**https://biorender.com**).

References

1 R. L. Siegel, K. D. Miller, N. S. Wagle and A. Jemal, *CA Cancer J. Clin.*, 2023, **73**, 17–48.
2 Z. J. Brown, D. I. Tsilimigras, S. M. Ruff, A. Mohseni, I. R. Kamel, J. M. Cloyd and T. M. Pawlik, *JAMA Surg.*, 2023, **158**, 410–420.
3 M. Reig, A. Forner, J. Rimola, J. Ferrer-Fàbrega, M. Burrel, Á. Garcia-Criado, R. K. Kelley, P. R. Galle, V. Mazzaferro, R. Salem, B. Sangro, A. G. Singal, A. Vogel, J. Fuster, C. Ayuso and J. Bruix, *J. Hepatol.*, 2022, **76**, 681–693.
4 Y. Yang, S. Qu, J. Li, C. Hu, M. Xu, W. Li, T. Zhou, L. Shen, H. Wu, J. Lang, G. Hu, Z. Luo, Z. Fu, S. Qu, W. Feng, X. Chen, S. Lin, W. Zhang, X. Li, Y. Sun, Z. Lin, Q. Lin, F. Lei, J. Long, J. Hong, X. Huang, L. Zeng, P. Wang, X. He, B. Zhang, Q. Yang, X. Zhang, J. Zou, W. Fang and L. Zhang, *Lancet Oncol.*, 2021, **22**, 1162–1174.
5 U. Harkus, M. Wankell, P. Palamuthusingam, C. McFarlane and L. Hebbard, *Semin. Cancer Biol.*, 2022, **86**, 799–815.
6 C. Lu, D. Rong, B. Zhang, W. Zheng, X. Wang, Z. Chen and W. Tang, *Mol. Cancer*, 2019, **18**, 130.
7 Y. Gao, M. You, J. Fu, M. Tian, X. Zhong, C. Du, Z. Hong, Z. Zhu, J. Liu, G. J. Markowitz, F. S. Wang and P. Yang, *J. Hepatol.*, 2022, **76**, 148–159.
8 D. G. Pellicci, H. F. Koay and S. P. Berzins, *Nat. Rev. Immunol.*, 2020, **20**, 756–770.
9 D. I. Godfrey, J. Le Nours, D. M. Andrews, A. P. Uldrich and J. Rossjohn, *Immunity*, 2018, **48**, 453–473.
10 C. Wang, X. Liu, Z. Li, Y. Chai, Y. Jiang, Q. Wang, Y. Ji, Z. Zhu, Y. Wan, Z. Yuan, Z. Chang and M. Zhang, *Sci. Rep.*, 2015, **5**, 14124.
11 P. J. Brennan, M. Brigl and M. B. Brenner, *Nat. Rev. Immunol.*, 2013, **13**, 101–117.
12 C. Gottschalk, E. Mettke and C. Kurts, *Front. Immunol.*, 2015, **6**, 379.
13 E. Y. Kim, H. Ner-Gaon, J. Varon, A. M. Cullen, J. Guo, J. Choi, D. Barragan-Bradford, A. Higuera, M. Pinilla-Vera, S. A. Short, A. Arciniegas-Rubio, T. Tamura, D. E. Leaf, R. M. Baron, T. Shay and M. B. Brenner, *J. Clin. Invest.*, 2020, **130**, 3238–3252.
14 Y. Qin, X. Bao and M. Zheng, *Front. Immunol.*, 2022, **13**, 1109347.
15 J. L. Matsuda, O. V. Naidenko, L. Gapin, T. Nakayama, M. Taniguchi, C. R. Wang, Y. Koezuka and M. Kronenberg, *J. Exp. Med.*, 2000, **192**, 741–754.
16 M. Li, D. Xie, X. Tang, C. Yang, Y. Shen, H. Zhou, W. Deng, J. Liu, S. Cai, L. Bai and Y. Wang, *Nano Lett.*, 2021, **21**, 6304–6313.
17 C. Ma, M. Han, B. Heinrich, Q. Fu, Q. Zhang, M. Sandhu, D. Agdashian, M. Terabe, J. A. Berzofsky, V. Fako, T. Ritz, T. Longerich, C. M. Theriot, J. A. McCulloch, S. Roy, W. Yuan, V. Thovarai, S. K. Sen, M. Ruchirawat, F. Korangy, X. W. Wang, G. Trinchieri and T. F. Greten, *Science*, 2018, **360**, eaan5931.
18 A. Sasakawa, T. Tatsumi, T. Takehara, S. Yamaguchi, M. Yamamoto, K. Ohkawa, T. Miyagi and N. Hayashi, *J. Hepatol.*, 2009, **50**, 1155–1162.
19 L. Van Kaer, *Nat. Rev. Immunol.*, 2005, **5**, 31–42.
20 X. Fan and A. Y. Rudensky, *Cell*, 2016, **164**, 1198–1211.
21 M.-X. Wu and Y.-W. Yang, *Adv. Mater.*, 2017, **29**, 1606134.
22 H. Zhang, Q. Li, R. Liu, X. Zhang, Z. Li and Y. Luan, *Adv. Funct. Mater.*, 2018, **28**, 1802830.
23 H. Zheng, Y. Zhang, L. Liu, W. Wan, P. Guo, A. M. Nyström and X. Zou, *J. Am. Chem. Soc.*, 2016, **138**, 962–968.
24 E. Boedtkjer and S. F. Pedersen, *Annu. Rev. Physiol.*, 2020, **82**, 103–126.
25 Q. Wang, Y. Sun, S. Li, P. Zhang and Q. Yao, *RSC Adv.*, 2020, **10**, 37600–37620.
26 Y. Chen, R. Lyu, J. Wang, Q. Cheng, Y. Yu, S. Yang, C. Mao and M. Yang, *Adv. Sci.*, 2023, **10**, e2302700.
27 J. Zhuang, C.-H. Kuo, L.-Y. Chou, D.-Y. Liu, E. Weerapana and C.-K. Tsung, *ACS Nano*, 2014, **8**, 2812–2819.

28 J. Shen, M. Ma, M. Shafiq, H. Yu, Z. Lan and H. Chen, *Angew. Chem., Int. Ed.*, 2022, **61**, e202113703.
29 K. Kurma, O. Manches, F. Chuffart, N. Sturm, K. Gharzeddine, J. Zhang, M. Mercey-Ressejac, S. Rousseaux, A. Millet, H. Lerat, P. N. Marche, Z. Macek Jilkova and T. Decaens, *Cancers*, 2021, **13**, 4981.
30 R. Verbeke, I. Lentacker, K. Breckpot, J. Janssens, S. Van Calenbergh, S. C. De Smedt and H. Dewitte, *ACS Nano*, 2019, **13**, 1655–1669.